# Tamm plasmon-polaritons in a metal coated porous silicon photonic crystal

Alexandre Juneau-Fecteau, Luc Frechette

Research Article | Vol. 8, No. 9 | 1 Sep 2018 | OPTICAL MATERIALS EXPRESS 2774
Optical Materials EXPRESS

# Tamm plasmon-polaritons in a metal coated porous silicon photonic crystal

ALEXANDRE JUNEAU-FECTEAU[1,2,*] AND LUC G. FRÉCHETTE[1,2]

[1] *Institut Interdisciplinaire d'Innovation Technologique (3IT), Université de Sherbrooke, 3000 Boulevard Université, Sherbrooke, J1K OA5, Québec, Canada*
[2] *Laboratoire Nanotechnologies Nanosystèmes (LN2) - CNRS UMI-3463, Université de Sherbrooke, 3000 Boulevard Université, Sherbrooke, J1K OA5, Québec, Canada*
[*] *alexandre.juneau.fecteau@usherbrooke.ca*

**Abstract:** We report the realization of a Tamm plasmon resonance in a planar structure by deposition of a gold film on a one-dimensional photonic crystal made of mesoporous silicon. The observation of a dip in the reflectance as well as a singularity in the ellipsometric angles confirms the presence of Tamm plasmon-polaritons with a higher quality factor than previously reported for porous Tamm structures. The simple electrochemical fabrication process of the porous silicon multilayer has the potential to facilitate the advent of integrated Tamm sensors by allowing an analyte to diffuse to the region where the electromagnetic field enhancement is highest while being low-cost and potentially CMOS-compatible.



## 1. Introduction

Tamm plasmon-polaritons (TPPs) are optical modes existing at the interface of a metal and a periodic dielectric multilayer known as a one-dimensional photonic crystal (PC) [1, 2]. Over the last decade, TPPs have been increasingly investigated as a promising alternative to surface plasmon-polaritons (SPPs) for the purpose of sensing [3], selective thermal emission [4, 5] and light generation [6]. Sensors utilizing the surface plasmon resonance on noble metals are now common place in biology, but because the SPP dispersion relation is outside the light cone those measurements are performed either with a coupling prism, also known as the Kretschmann-Raether configuration, or with a grating etched in the metal [7]. Both approaches are difficult to implement in high-throughput microarray experiments since they are performed at a large oblique angle of incidence [8]. A sensor based on the Tamm resonance is an obvious solution to this problem since the dispersion relations lies entirely within the light cone for both TE and TM polarizations. Measurements can thus be performed at normal incidence without patterning of the surface. However, while the high-intensity electric field of SPPs extends into free space above the metal, the electric field of the TPPs is localized within the PC where it is not easily accessible. Therefore, a method must be devised to infiltrate the analyte inside the layered structure. Zhang et al. proposed a PC made of dielectric layers separated by air [9]. Because the fabrication of such a device would require multiple sacrificial layers to achieve the several sub-micron gaps, it would be vulnerable to problems like adhesion between the suspended membranes, mechanical stability and deformation from residual stresses. Auguié et al. opted for a different approach by fabricating the PC with porous layers of $SiO_2$ and $TiO_2$ in contact with a Au film and were able to demonstrate detection of organic solvents from a wavelength shift of the resonance [10]. Alternatively, porous Si (PSi) is a very interesting option for this application due to the ease of porosification in a single electrochemical process and the wide range of refractive indices that can be obtained by changing the porosity. A high specific surface, which can reach more than 300 $m^2/cm^3$ depending on fabrication conditions [11], has made PSi a prime candidate for biosensing [12, 13]. Finally, the preponderance of Si in the microelectronic industry and the fact that PSi can be integrated with CMOS electronics offers a significant advantage over competing materials [14].

#336484 https://doi.org/10.1364/OME.8.002774
Journal © 2018 Received 29 Jun 2018; revised 9 Aug 2018; accepted 10 Aug 2018; published 20 Aug 2018

Optical Materials EXPRESS

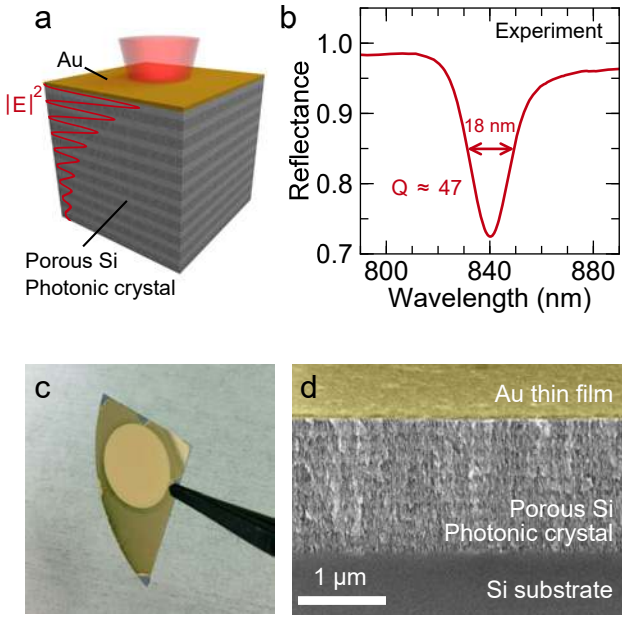


Fig. 1. (a) Schematic of the Au coated PSi multilayer. (b) Measured reflectance at normal incidence of the Au thin film on the PSi PC. (c) Photography and (d) scanning electron microscope cross-section of the fabricated sample.

In this work, we used PSi to fabricate the PC in a Tamm structure (Fig. 1a). This nanomaterial is particularly well-suited for the fabrication of a PC since multilayers can be easily created by periodically changing the current during porosification [15]. The presence of Bloch surface waves on PSi PC was previously used for vapor sensing [16, 17] and it was recently demonstrated that metal nanoparticles fabricated on a such a structure greatly enhance Raman scattering due to the high electric field confinement [18]. We observed a dip in the measured reflectance of a PSi PC coated with gold (Fig. 1b), which we explain as a signature of the Tamm resonance using an analytical model for 1D electromagnetic waves. The width of this resonance, related to the quality factor, is of first importance for sensing applications since it determines the sensitivity of the structure to a change in refractive index within the PC. As will be presented, the measured quality factor of the fabricated device is superior than for previous experimental demonstrations of TPPs in the same wavelength range.

## 2. Fabrication and modeling

We fabricated the PSi PC through electrochemical anodization at room temperature of $p^+$-doped Si (100) with resistivity of 0.01 Ωcm using a 1:1 solution of 49% HF and ethanol as the electrolyte. The periodicity of the multilayer was achieved by alternating between two current densities, 53 mA/cm$^2$ and 184 mA/cm$^2$, for the low and high porosity layers with the finished structure containing 10 pairs of the two layer types. The associated porosities, obtained through gravimetric measurements of single layers, are (43 ± 1)% and (59 ± 1)% and the expected thicknesses 82 nm and 105 nm respectively. Pauses of 8 s between each pulse and mechanical agitation ensured a proper mixing of the electrolyte throughout the process. The PSi multilayer was then rinsed in ethanol and dried in nitrogen. A thin film of Au was evaporated on the surface with a thickness of (46 ± 3) nm according to stylus profilometry. A picture of the resulting Au coated PC is shown on

Optical Materials EXPRESS

Fig. 1(c) and a scanning electron microscope cross-section of the structure on Fig. 1(d). Using a Filmetrics F10-RT-EXR spectrometer, we measured the reflectance of the PC before and after Au evaporation, as well as from the metal film on a part of the Si substrate that was not porosified.

In order to simulate the propagation of electromagnetic waves in the multilayer, we need to model how the porosity affects the optical properties of PSi. We can approximate the layers as homogeneous since the wavelength of visible light is at least an order of magnitude larger than the pore size of mesoporous Si [11], but we must still take absorption and dispersion into account. The Bruggeman effective medium model [21] provides a simple way to compute the effective dielectric function ($\varepsilon_{\mathrm{PSi}}$) of the PSi layers from the complex dielectric function of bulk Si ($\varepsilon_{\mathrm{Si}}$) and the porosity ($P$):

$$(1-P)\frac{\varepsilon_{\mathrm{Si}}-\varepsilon_{\mathrm{PSi}}}{\varepsilon_{\mathrm{Si}}+2\varepsilon_{\mathrm{PSi}}}+P\frac{\varepsilon_{\mathrm{air}}-\varepsilon_{\mathrm{PSi}}}{\varepsilon_{\mathrm{air}}+2\varepsilon_{\mathrm{PSi}}}=0. \tag{1}$$

Given the experimental values of $\varepsilon_{\mathrm{Si}}$ reported by Green [19], the refractive indices $n_{\mathrm{PSi}} = \mathrm{Re}(\sqrt{\varepsilon_{\mathrm{PSi}}})$ and extinction coefficients $\kappa_{\mathrm{PSi}} = \mathrm{Im}(\sqrt{\varepsilon_{\mathrm{PSi}}})$ of PSi are plotted on Figs. 2(a)-2(b) for both porosities used in this study. We designed the PC so that each PSi layer has a quarter-wavelength thickness of $\lambda_0/4n_i$, where $\lambda_0 \approx 800$ nm is the center of the PC bandgap and $n_i$ the refractive index at $\lambda_0$. For the gold film, we used the refractive index ($n_{\mathrm{Au}}$) and extinction coefficient ($\kappa_{\mathrm{Au}}$) measured by Olmon et al [20]. The Tamm resonance arises when a PC is placed next to a material where the real part of the dielectric function is negative. Using

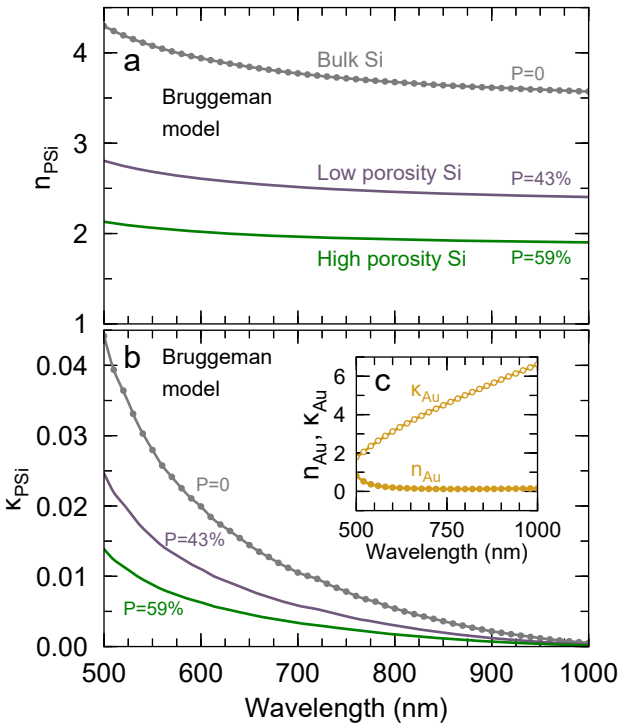


Fig. 2. (a) Effective refractive indices and (b) extinction coefficients of the high and low porosity PSi layers (green and purple) calculated using Bruggeman model and the experimental data for bulk Si (gray) provided by Green [19]. (c) Refractive index (full circles) and extinction coefficient (open circles) of Au measured by Olmon et al [20].

Optical Materials EXPRESS

$\varepsilon_{Au} = (n_{Au} + i\kappa_{Au})^2$, simple algebra shows that $\mathrm{Re}(\varepsilon_{Au}) < 0$ when $\kappa_{Au} > n_{Au}$. We see on Fig. 2(c) that this is the case for wavelengths from 500 to 1000 nm.

## 3. Results and discussion

Figure 3(a) shows the measured reflectance spectra of the Au film deposited on bulk Si and of the PSi multilayer before and after deposition. The PSi structure has a photonic stop-band leading to near perfect reflectance for the selected wavelength range. Both the Au film and the PC are almost perfect mirrors in this region, but their superposition is not since the reflectance drops around 840 nm when Au is present on the PC. We can demonstrate that this phenomenon is a manifestation of TPPs by simulating the complex reflection coefficients $r_{Au}$ and $r_{PC}$ of the Au film and PC with the scattering matrix method [22]. A simple criterion for the existence of the Tamm resonance is the condition $r_{Au}r_{PC} = 1$ [1]. Thus, TPPs exist at the wavelength where the modulus of the complex product $r_{Au}r_{PC}$ is unity while its phase reaches zero. Figure 3(b) shows that this occurs at 852 nm, very close to the dip in the measured reflectance of the Tamm structure. Based on the full width at half maximum (FWHM) of the resonance, the quality factor is 47, higher than 12 in the mesoporous device fabricated by Auguié et al. [10] and 29 for the Tamm resonance measured by Afinogenov et al. [23] in a non-porous multilayer. The most interesting property of TPPs for applications, namely that their dispersion relation lies within the light cone, can be illustrated by plotting the reflectance as a function of energy and the in-plane wavevector ($k_{\parallel}$), as seen on Fig. 3(c). As previously reported [1], the dispersion relation of TPPs follows the quadratic equation:

$$E_{TPP} = \frac{\hbar^2}{2m} k_{\parallel}^2 + E_0. \tag{2}$$

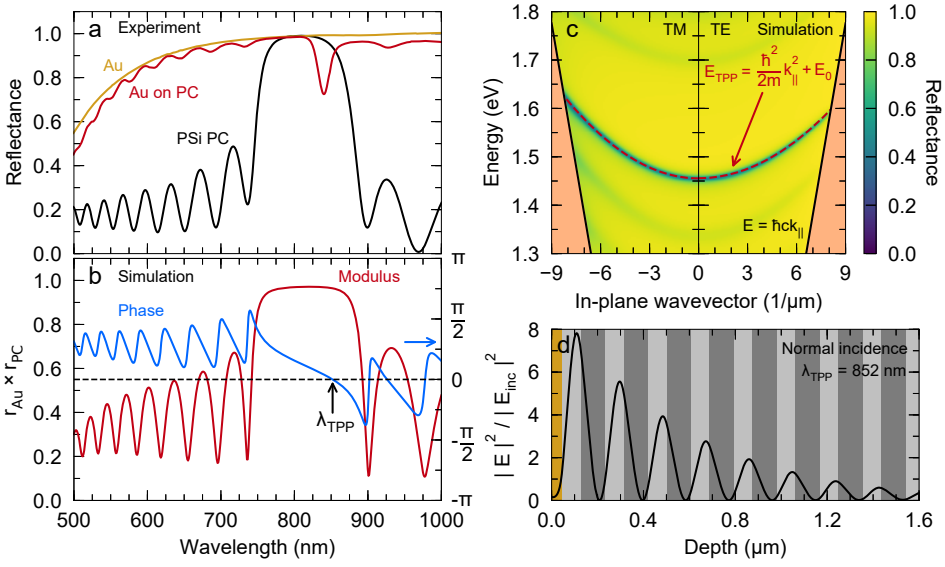


Fig. 3. (a) Normal incidence reflectance of the Au on PC multilayer. (b) Product of the calculated complex reflection coefficients for the air/Au and air/PC at normal incidence. (c) Simulated reflectance with quadratic fits of the dispersion relations of the Tamm resonance (red dashed lines) for both TE and TM polarizations. (d) Normalized electric field of the localized resonance at normal incidence.

Optical Materials EXPRESS

The effective masses ($m$) obtained from fits are $1.76 \times 10^{-5} m_0$ and $1.52 \times 10^{-5} m_0$ for the TE and TM polarizations respectively, where $m_0$ is the free electron mass.

A key insight to gain from the simulations is the distribution of the electric field inside the multilayer. We see on Fig. 3(d) a factor 8 of enhancement in the field intensity at the resonant wavelength for normal incidence. The fact that the energy is localized inside the PC validates the use of a porous material for its fabrication, provided the analyte can traverse the Au barrier to reach this region of high intensity. The metal film could itself be made porous or holes could be etched in the surface for this purpose. Another possibility is to detach the PSi PC using electropolishing [24]. The flexible freestanding multilayer can then be placed on a metal substrate so that it can be infiltrated from the top with the solution to test.

Interestingly, the Tamm resonance is associated with a change in the geometric phase between two photonic bands and is topologically protected [25]. To illustrate this point, let us consider a PC made by a repetition of layer A with properties ($n_A = 2.5$, $d_A = 100$ nm) and layer B with ($n_B = 1.9$, $d_B = 100$ nm) in a symmetric unit cell centered around layer B. We neglect absorption and dispersion of the refractive indices of PSi and use average values instead to simplify band structure calculations. Figure 4(a) shows the band structure of the PC calculated using the S-matrix method [26]. The simulated reflectance of 10 unit cells is plotted on Fig. 4(b) and the reflection phase $\phi_{PC}$ on Fig. 4(c). The first three bands are isolated from each other by bandgaps where reflectance is high. The geometric phase of bulk bands in a 1D photonic crystal, also known as Zak phase, can be either 0 or $\pi$ with the value given by [27, 28]:

$$\exp\left(i\theta_0^{\text{Zak}}\right) = \text{sgn}\left[1 - \varepsilon_a \mu_b / (\varepsilon_b \mu_a)\right] \tag{3}$$

$$\exp\left(i\theta_n^{\text{Zak}}\right) = -\text{sgn}\left(\phi_n\right) / \text{sgn}\left(\phi_{n-1}\right) \qquad \text{for } n > 0 \tag{4}$$

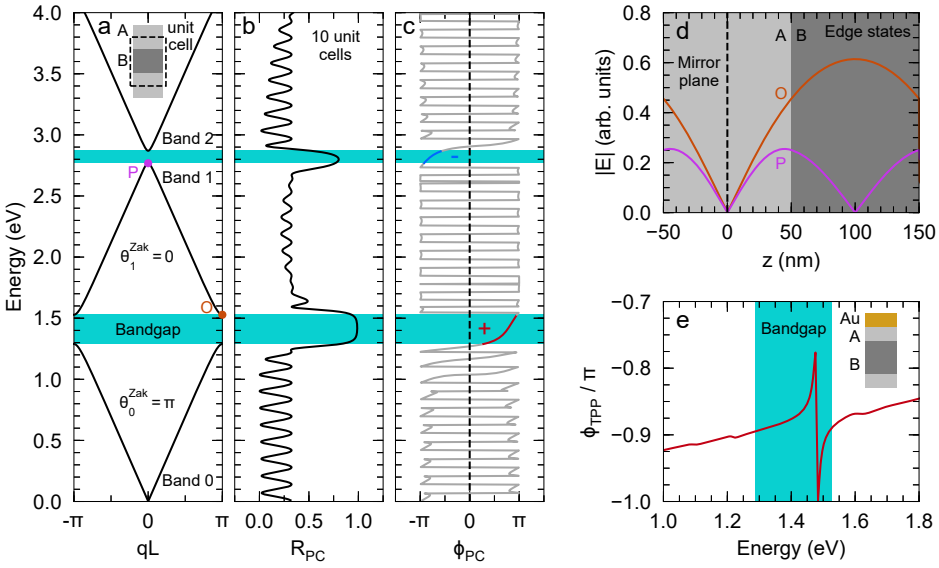


Fig. 4. (a) Band structure of a PC with a symmetric unit cell of length $L = d_A + d_B$ with $d_A = d_B = 100$ nm and refractive indices $n_A = 2.5$ and $n_B = 1.9$. The Bloch wavevector $q$ is perpendicular to the layers. (b) Simulated reflectance of 10 unit cells of the PC and (c) reflection phase showing opposite signs in the two bandgaps. (d) Electric field amplitude of the edge states of band 1. (e) Reflection phase of the PC coated with 46 nm of gold.

Optical Materials EXPRESS

where $\phi_n$ and $\phi_{n-1}$ are the reflection phases in the bandgaps above and below the $n$th band. The Zak phase of band 0 is $\theta_0^{\text{Zak}} = \pi$ because $\varepsilon_a > \varepsilon_b$ and the materials are not magnetic so $\mu_a = \mu_b = 1$. The Zak phase of band 1, however, is $\theta_1^{\text{Zak}} = 0$ since $\phi_{\text{PC}}$ takes opposite signs in the two bandgaps. Thus, there is a change of Zak phase from band 0 to band 1. Another way to infer $\theta_1^{\text{Zak}}$ is to compare the symmetry of the low and high energy edge states on both sides of band 1 as plotted on Fig. 4(d). If the electric fields at the edges have the same odd or even symmetry with respect to the origin of the unit cell, the Zak phase of the band is 0. It is $\pi$ otherwise [27]. In the case of band 1, the symmetry is odd in both edge states because $E(z) = -E(-z)$ requires $|E(0)| = 0$, meaning that $\theta_1^{\text{Zak}}$ must be 0. This discontinuity in Zak phase introduces an interface state in the gap between the first two bands when a metal is deposited on the PC. This mode is the Tamm resonance and creates a jump in the reflection phase within the bandgap as shown on Fig. 4(e).

A common way to achieve sensing with TPPs is to measure the shift in reflectance or transmittance of the Tamm structure at normal incidence due to the presence of a given analyte, but it was recently demonstrated that the sensitivity is higher when measuring directly the reflection phase change using an ellipsometer [29]. This is possible since the ellipsometric angles $\Psi$ and $\Delta$ are related to the reflection coefficients for the TE and TM polarizations by the relation $\tan(\Psi)e^{i\Delta} = r_{\text{TM}}/r_{\text{TE}}$. Such a measurement requires an oblique angle of incidence since both polarization states are indistinguishable at normal incidence, but it can also be performed in the far-field without a prism or grating due to the ability of TPPs to couple with propagative light at any angle. The highest sensitivity provided by this phase-based approach might be preferable in some applications. Therefore, we studied the Tamm resonance in the fabricated structure at the incidence angle $\theta = 70°$ with a J. A. Woollam alpha-SE ellipsometer. The angle $\Psi$ (Fig. 5(a)) reaches a minimum at the wavelength where the phase $\Delta$ (Fig. 5(b)) exhibits a jump associated with the resonance as predicted by the simulations presented on Figs. 5(c)-5(d). The

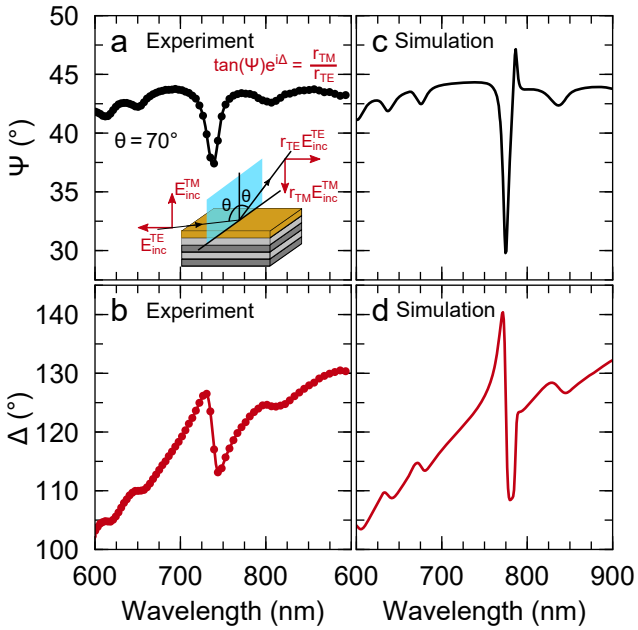


Fig. 5. Measured ellipsometric angles of the Au on PC multilayer (a and b) compared to simulations (c and d). The Tamm resonance is visible as a dip in the amplitude ratio $\Psi$ and a jump in the phase difference $\Delta$.

dip occurs at a lower wavelength than normal incidence as suggested by the dispersion relation on Fig. 3(c). We attribute the discrepancy between the measured and simulated curves to the surface roughness and fabrication defects such as inhomogeneities in thickness and porosity of the PSi layers. Lowering the electrolyte temperature would reduce layer roughness and increase control of the PSi properties [30], possibly improving the agreement with the theoretical model as well as the quality factor.

## 4. Conclusion

In summary, we have demonstrated the existence of a Tamm resonance in a gold-coated multilayer made of mesoporous Si through reflectometry and ellipsometry. This unique type of surface waves can be excited by propagative light at any angle and for both polarizations because its parabolic dispersion relation exists entirely within the light cone. The measured quality factor at normal incidence is superior to the state of the art Tamm structures made of porous layers. According to simulations, the incident electric field intensity is increased by a factor of 8 by the resonance. The use of a porous material is of crucial importance for sensing applications since the strong electromagnetic field enhancement is localized within the PC. The whole dielectric multilayer is fabricated at a low cost in an electrochemical cell by simply varying the current during the porosification of Si. Since gold could be replaced by other metals like aluminum, this process is also potentially CMOS-compatible.

## References

1. M. Kaliteevski, I. Iorsh, S. Brand, R. A. Abram, J. M. Chamberlain, A. V. Kavokin, and I. A. Shelykh, "Tamm plasmon-polaritons: Possible electromagnetic states at the interface of a metal and a dielectric Bragg mirror," Phys. Rev. B **76**, 165415 (2007).
2. M. E. Sasin, R. P. Seisyan, M. A. Kalitteevski, S. Brand, R. A. Abram, J. M. Chamberlain, A. Y. Egorov, A. P. Vasil'ev, V. S. Mikhrin, and A. V. Kavokin, "Tamm plasmon polaritons: Slow and spatially compact light," Appl. Phys. Lett. **92**, 251112 (2008).
3. R. Badugu, E. Descrovi, and J. R. Lakowicz, "Radiative decay engineering 7: Tamm state-coupled emission using a hybrid plasmonic–photonic structure," Anal. Biochem. **445**, 1–13 (2014).
4. Z.-Y. Yang, S. Ishii, T. Yokoyama, T. D. Dao, M.-g. Sun, T. Nagao, and K.-p. Chen, "Tamm plasmon selective thermal emitters," Opt. Lett. **41**, 4453–4456 (2016).
5. Z.-Y. Yang, S. Ishii, T. Yokoyama, T. D. Dao, M.-G. Sun, P. S. Pankin, I. V. Timofeev, T. Nagao, and K.-P. Chen, "Narrowband Wavelength Selective Thermal Emitters by Confined Tamm Plasmon Polaritons," ACS Photonics **4**, 2212–2219 (2017).
6. A. Jiménez-Solano, J. F. Galisteo-López, and H. Míguez, "Flexible and Adaptable Light-Emitting Coatings for Arbitrary Metal Surfaces based on Optical Tamm Mode Coupling," Adv. Opt. Mater. **6**, 1700560 (2018).
7. J. Homola, "Surface Plasmon Resonance Sensors for Detection of Chemical and Biological Species," Chem. Rev. **108**, 462–493 (2008).
8. A. J. Haes and R. P. Van Duyne, "A Nanoscale Optical Biosensor: Sensitivity and Selectivity of an Approach Based on the Localized Surface Plasmon Resonance Spectroscopy of Triangular Silver Nanoparticles," J. Am. Chem. Soc. **124**, 10596–10604 (2002).
9. W. L. Zhang, F. Wang, Y. J. Rao, and Y. Jiang, "Novel sensing concept based on optical Tamm plasmon," Opt. Express **22**, 14524 (2014).
10. B. Auguié, M. C. Fuertes, P. C. Angelomé, N. L. Abdala, G. J. A. A. Soler Illia, and A. Fainstein, "Tamm Plasmon Resonance in Mesoporous Multilayers: Toward a Sensing Application," ACS Photonics **1**, 775–780 (2014).
11. J. Salonen, M. Björkqvist, E. Laine, and L. Niinistö, "Effects of Fabrication Parameters on Porous p+-Type Silicon Morphology," physica status solidi (a) **182**, 249–254 (2000).
12. V. S.-Y. Lin, K. Motesharei, K.-P. S. Dancil, M. J. Sailor, and M. R. Ghadiri, "A Porous Silicon-Based Optical Interferometric Biosensor," Science **278**, 840–843 (1997).
13. F. Cunin, T. A. Schmedake, J. R. Link, Y. Y. Li, J. Koh, S. N. Bhatia, and M. J. Sailor, "Biomolecular screening with encoded porous-silicon photonic crystals," Nat. Mater. **1**, 39–41 (2002).
14. G. Barillaro, P. Bruschi, F. Pieri, and L. M. Strambini, "CMOS-compatible fabrication of porous silicon gas sensors and their readout electronics on the same chip," physica status solidi (a) **204**, 1423–1428 (2007).
15. G. Vincent, "Optical properties of porous silicon superlattices," Appl. Phys. Lett. **64**, 2367–2369 (1994).
16. E. Guillermain, V. Lysenko, and T. Benyattou, "Surface wave photonic device based on porous silicon multilayers," J. Lumin. **121**, 319–321 (2006).
17. F. Michelotti, B. Sciacca, L. Dominici, M. Quaglio, E. Descrovi, F. Giorgis, and F. Geobaldo, "Fast optical vapour sensing by Bloch surface waves on porous silicon membranes," Phys. Chem. Chem. Phys. **12**, 502–506 (2010).

Optical Materials EXPRESS


18. M. Fränzl, S. Moras, O. D. Gordan, and D. R. T. Zahn, "Interaction of One-Dimensional Photonic Crystals and Metal Nanoparticle Arrays and Its Application for Surface-Enhanced Raman Spectroscopy," The J. Phys. Chem. C **122**, 10153–10158 (2018).
19. M. A. Green, "Self-consistent optical parameters of intrinsic silicon at 300k including temperature coefficients," Sol. Energy Mater. Sol. Cells **92**, 1305–1310 (2008).
20. R. L. Olmon, B. Slovick, T. W. Johnson, D. Shelton, S.-H. Oh, G. D. Boreman, and M. B. Raschke, "Optical dielectric function of gold," Phys. Rev. B **86**, 235147 (2012).
21. J. Volk, T. L. Grand, I. Bársony, J. Gombkötő, and J. J. Ramsden, "Porous silicon multilayer stack for sensitive refractive index determination of pure solvents," J. Phys. D: Appl. Phys. **38**, 1313 (2005).
22. D. M. Whittaker and I. S. Culshaw, "Scattering-matrix treatment of patterned multilayer photonic structures," Phys. Rev. B **60**, 2610–2618 (1999).
23. B. I. Afinogenov, V. O. Bessonov, A. A. Nikulin, and A. A. Fedyanin, "Observation of hybrid state of Tamm and surface plasmon-polaritons in one-dimensional photonic crystals," Appl. Phys. Lett. **103**, 061112 (2013).
24. M. Ghulinyan, C. J. Oton, G. Bonetti, Z. Gaburro, and L. Pavesi, "Free-standing porous silicon single and multiple optical cavities," J. Appl. Phys. **93**, 9724 (2003).
25. S. V. Boriskina and Y. Tsurimaki, "Sensitive singular-phase optical detection without phase measurements with Tamm plasmons," J. Physics: Condens. Matter **30**, 224003 (2018).
26. Z.-Y. Li and L.-L. Lin, "Photonic band structures solved by a plane-wave-based transfer-matrix method," Phys. Rev. E **67**, 046607 (2003).
27. M. Xiao, Z. Zhang, and C. Chan, "Surface Impedance and Bulk Band Geometric Phases in One-Dimensional Systems," Phys. Rev. X **4**, 021017 (2014).
28. Q. Wang, M. Xiao, H. Liu, S. Zhu, and C. T. Chan, "Measurement of the Zak phase of photonic bands through the interface states of a metasurface/photonic crystal," Phys. Rev. B **93**, 041415 (2016).
29. Y. Tsurimaki, J. K. Tong, V. N. Boriskin, A. Semenov, M. I. Ayzatsky, Y. P. Machekhin, G. Chen, and S. V. Boriskina, "Topological Engineering of Interfacial Optical Tamm States for Highly Sensitive Near-Singular-Phase Optical Detection," ACS Photonics **5**, 929–938 (2018).
30. S. Setzu, G. Lérondel, and R. Romestain, "Temperature effect on the roughness of the formation interface of p-type porous silicon," J. Appl. Phys. **84**, 3129–3133 (1998).